## PAPER

# Highly sensitive detection of low-level water content in organic solvents and cyanide in aqueous media using novel solvatochromic AIEE fluorophores†

Wei Chen,[a] Zhiyun Zhang,[a] Xin Li,*[b] Hans Ågren[b] and Jianhua Su*[a]

A great deal of effort has been devoted to develop easy-to-use fluorescent probes for detecting analytes due to their advantages in the field of chemo- and bio-sensing. Herein, two novel 2,2′-biindenyl-based derivatives **BDM** and **BDBM** containing dicyanovinyl groups have been designed and synthesized, and are shown to possess the remarkable dual properties of solvatochromism and aggregation-induced emission enhancement (AIEE). Importantly, both of them are found to serve as fluorescent indicators for the qualitative and quantitative detection of low-level water in organic solvents. Meanwhile, both **BDM** and **BDBM** emit yellowish orange and orange fluorescence, respectively, in their aggregated states. Furthermore, with dicyanovinyl groups as the recognition sites, both compounds can act as colourimetric and fluorescent sensors for highly sensitive and selective detection of cyanide in aqueous media, and the apparent response signals can be observed by the naked eye even in the presence of various interference anions, promising practical applications for detecting cyanide in drinking water. Besides, optical spectroscopic techniques, NMR titration measurements, and density functional theory calculations are conducted to rationalize the sensing mechanisms of the two probes.

## Introduction

Development of luminogens whose aggregates emit more efficiently than in solution has triggered much interest in recent years. Tang's group in 2001 first reported this unusual phenomenon, which is exactly opposite to the aggregation-caused quenching (ACQ) effect, and coined it "aggregation-induced emission" (AIE).[1] In 2002, the group of Park also observed the phenomenon of aggregation-induced emission enhancement (AIEE).[2] Since then, luminogens with AIE(E) properties have been intensively studied, including varieties of proposed mechanisms and potential applications. To date, a large number of molecules with AIE(E) properties have been developed and extensively used in organic light-emitting diodes (OLEDs),[3,4] supramolecular polymers,[5] bio/chemosensors,[6,7] drug delivery,[8,9] two-photon absorption (2PA) materials,[10,11] and more. Previously, our group reported a series of novel 2,2′-

biindenyl-based AIE fluorophores with tunable solid-state emission, which cover the whole visible region.[12] That work motivated us to pursue further design of functional materials utilizing biindenyl-based AIE molecules. In this work it is our intention to utilize the biindenyl functional group as a building block for smart materials with applications in chemo- and biosensing. We aim to modify the biindenyl-based chromophores to form stimuli-responsive compounds with pronounced solvatochromic effect, which might offer novel chemo- or biosensors for detecting metal cations, toxic anions, biomolecules, explosives, *etc.*

Qualitative and quantitative detection of low-level water as impurities in organic solvents is also of great significance in several fields of chemistry and industry processes such as pharmaceutical manufacturing, food processing, paper production, biomedical and environmental monitoring.[13] Although there exist extensive traditional methods for quantification of humidity in gas or liquid phases, which feature high sensitivity and which might be applicable to a large variety of samples, these methods also have some drawbacks: for instance, time-consuming, costly and involving sophisticated instruments. Recently, optical sensors for water sensing have drawn considerable attention due to the flexibility in readout, the possibility of remote and *in situ* monitoring as well as the ease and low-cost of fabrication.[14,15] In particular, fluorescence methods, such as lifetime, intensity and wavelength ratiometric

[a] Key Laboratory for Advanced Materials and Institute of Fine Chemicals, East China Universtity of Science & Technology, Shanghai 200237, P. R. China. E-mail: bbsjh@ecust.edu.cn; Fax: +86-21-64252288

[b] Division of Theoretical Chemistry and Biology, School of Biotechnology, KTH Royal Institute of Technology, SE-10691 Stockholm, Sweden. E-mail: lixin@theochem.kth.se

† Electronic supplementary information (ESI) available: Photophysical data, crystal data, theoretical calculated data, ^{1}H and ^{13}C NMR spectra and ESI-TOF mass spectra of **BDM** and **BDBM**. CCDC 1016979. For ESI and crystallographic data in CIF or other electronic format see DOI: 10.1039/c4ra15199b

sensing approaches, have been widely investigated and applied for the detection of water content in organic solvents.[16–22]

Cyanide has been continuously of concern all over the world due to its high toxicity and widespread use in industrial processes such as acrylic fiber manufacturing, metallurgy, herbicide production, and silver or gold extraction.[23,24] Uptake of toxic cyanide could occur through absorption by lungs, exposure to skin, and also from contaminated food and polluted drinking water.[23–25] Trace amount of cyanide can directly lead to the death of human beings in several minutes because it strongly binds to the active site of cytochrome-c, disrupting the mitochondrial electron-transport chain and inhibiting cellular respiration in mammalian cells.[26] The World Health Organization (WHO) has set the maximum permissive level of cyanide in drinking water as 1.9 μmol L$^{-1}$ to prevent poisoning.[27] Therefore, it is of great significance to find convenient and efficient detection methods at the environmental and biological levels. Among various approaches for the detection of cyanide such as electrochemical analysis, ion chromatography and the involvement of intelligent instruments,[28] optical sensors show considerable advantage over others for their simplicity, convenience and low-cost of implementation. The sensing process is often accompanied by changes in absorption or fluorescence spectra that can be precisely monitored and in some cases detectable by naked eye. To minimize the interference of other anions, cyanide chemodosimeters take advantage of the unique nucleophilicity of cyanide to realize recognition through the bond-formation reaction between the probing molecule and cyanide anions.[29] Nevertheless, since the presence of water will weaken the nucleophilic addition reaction of cyanide,[30,31] most of the chemodosimeters need to be operated either in pure organic solvents or a mixture of organic and aqueous solvent, which largely restricts their practical applications.[32,33] To date, reports relating sensors that recognized cyanide in complete water have been scarce.[34–39] We believe that there is large room for improvement in terms of sensitivity and applicability, and that it thereby is important to develop effective chemosensors for detection of cyanide in aqueous media.

Herein, two novel probes **BDM** and **BDBM** have been designed and synthesized, as shown in Scheme 1. In the molecular design, the dicyanovinyl group was introduced because it can act not only as a strong withdrawing group to induce an intramolecular charge transfer (ICT) transition but also as a cyanide reactive unit.[40–47] It is thus expected that these two compounds possess intense ICT effects, which bestow the derivatives with pronounced solvatochromism.[48] In addition, the nucleophilic attack of cyanide at the α-position of the dicyanovinyl group would improve their water solubility and lead to significant changes in fluorescence and absorption, enabling them as practical reaction-based cyanide sensors in aqueous media.[33] Indeed, the two indicators inherit the AIE characterization and nonplanar distortion from the mother compound 1,1,1′,1′-tetramethyl-3,3′-diphenyl-2,2′-biindanyl, and exhibit highly efficient red emission in the solid state with quantum yields of 24% and 22%, respectively. More importantly, both compounds can serve as excellent fluorescent indicators for the detection of low-level water content in THF or
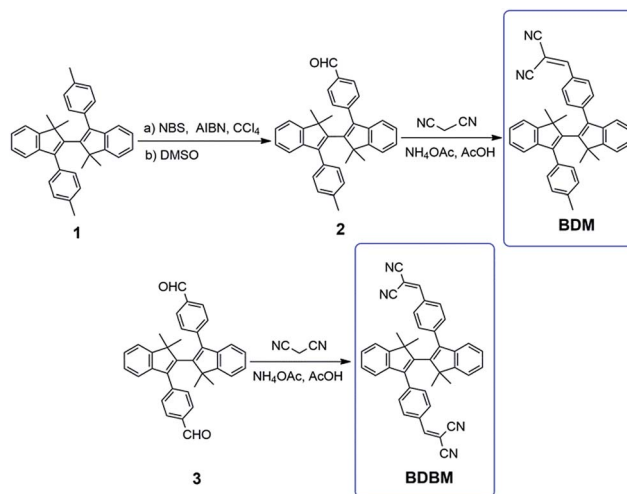


**Scheme 1** Chemical structures and synthetic routes of compounds **BDM** and **BDBM**.

dioxane as well as the detection of cyanide in water (containing 1% DMSO) under the assistance of cetyltrimethylammonium bromide (CTAB).[49] These facts motivate research on multifunctional biindenyl-based fluorophores acting as indicators for the detection of water content and cyanide anions. Furthermore, our sensing systems effectively avoid the negative effect of water on specific cyanide reactions due to the presence of CTAB, promising their practical applications for detecting cyanide in drinking water.

## Results and discussion

### Synthesis

The synthetic routes of compounds **BDM** and **BDBM** are shown in Scheme 1, and the key compounds **2** and **3** were synthesized according to the literature.[12] Mono- or dibromination of **1** gave the corresponding benzyl bromide, which was heated in dimethylsulfoxide (DMSO) to afford **2** or **3**. After subsequent Knoevenagel reaction with excess malononitrile, the desired products were obtained. Both target compounds were carefully characterized by proton and carbon nuclear magnetic resonance spectroscopy ($^1$H NMR, $^{13}$C NMR) and high resolution mass spectroscopy (HRMS) (see the ESI† for the details).

### Solvatochromic effect

The photophysics of the D−π−A conjugates in solution strongly depends on the solvent polarity.[50] Due to the presence of electron-withdrawing dicyanovinyl groups, **BDM** and **BDBM** possess typical D−π−A structures. Thus, we firstly studied their spectral properties in solution, and the results are summarized in Table S1.† As shown in Fig. S1a,† the absorption spectra of **BDM** display minor changes in different solvents. In contrast, as the solvent polarity increased (from *n*-hexane to acetonitrile), the emission bands of **BDM** gradually red-shifted from 537 nm to 637 nm because of the dipole–dipole interactions between the solute and solvents,[51] exhibiting a remarkable

bathochromic effect (Fig. 1a and Table S1†). Meanwhile, a notable reduction in the fluorescence quantum yield ($\Phi_F$) was observed. The maximum of the emission bands shifted significantly to lower energy region, accompanied by a broadening of the emission bands in polar solvents, which indicates an ICT character for the excited state.[52] Results shown in the absorption and fluorescence spectra imply that the combination of the electron-donating biindene and the electron-withdrawing dicyanovinyl group offers ICT process in the molecule and that the absorption bands at around 400 nm arise from ICT transition.

When the second dicyanovinyl groups was introduced into biindene to give **BDBM**, the maximum of the absorption band was blue-shifted from 407 nm to 400 nm in cyclohexane compared with **BDM** (Table S1†). The existence of two dicyanovinyl groups may be responsible for the hypochromic shift because dicyanovinyl group as a strong electron-withdrawing group weakens the electron-donating ability of biindene. With further increase of solvent polarity, the absorption peaks were hardly changed, while the emission bands showed gradual redshifting, similar to that of **BDM** (Fig. S1b† and 1b). Under UV irradiation, the emission can be finely tuned from green to red by changing the solvent from *n*-hexane to acetonitrile (Fig. 1d).

To evaluate the solvatochromism of the two compounds, the relationship between the solvent orientation polarizability ($\Delta f$) and the Stokes shift ($\Delta \nu$) was studied using the Lippert–Mataga equation.[53] From the $\Delta \nu$–$\Delta f$ plots (Fig. S2a†) it is found that the slopes of the fitting lines for **BDM** and **BDBM** are as large as 12 021.6 and 8613.3, respectively. In comparison with 9347.7 for a tetraphenylethene derivative (TPEBM),[26] the slope of the fitting line for **BDM** is much larger, implying **BDM** possesses strong solvatochromism. The slope of the fitting line for **BDM** is much larger than **BDBM**, suggesting that the ICT effect of the former is more pronounced than the latter. In both compounds, the excited state has a larger dipole moment than the ground state, owing to the substantial charge redistribution during the ICT-type excitation, which originates from the relaxation of the initially formed Frank–Condon excited state, instead of the

direct transition from the ground state.[54] The excited states are therefore better stabilized by the polar solvents compared with their respective ground states, explaining the observed substantial solvatochromism of both compounds. This provides a good evidence for the two compounds to act as a suitable solvent polarity indicators.

To elucidate the influence of the geometric and electronic structure of **BDM** and **BDBM** on solvatochromism, we conducted theoretical calculations. The electronic structures of **BDM** and **BDBM** exhibit differences owing to the difference in their chemical structures. As shown in Fig. S3,† the energy levels of the HOMO and LUMO of **BDM** are higher than those of **BDBM**, and **BDM** has a narrower HOMO–LUMO gap. Interestingly, the LUMO and LUMO + 1 of **BDBM** reside in similar energy levels, while in **BDM** the energy levels of LUMO and LUMO + 1 differ from more than 1 eV. Contour plots of the frontier molecular orbitals (Fig. 2) reveal that the HOMO is located on the central indene rings in both **BDM** and **BDBM**; however, the LUMO and LUMO + 1 of these two compounds are quite different. In **BDBM**, both LUMO and LUMO + 1 are located on the peripheral phenyl rings with dicyanovinyl substitutions, while in **BDM** the LUMO exclusively reside on the only dicyanovinyl-substituted phenyl branch. The LUMO + 1 of **BDM** is located on the central indene rings instead of peripheral phenyl rings. This leads to the very different characteristics in the excited states of **BDM** and **BDBM**.

Time-dependent density functional (TD-DFT) calculations provide further insight into the excited states of the two compounds. As shown in Table S2,† the lowest excited states ($S_1$) of both **BDM** and **BDBM** correspond to HOMO → LUMO transitions. Owing to the different composition of the frontier molecular orbitals, the intramolecular charge transfer from the central indene rings to the dicyanovinyl-substituted phenyl branches is estimated as $0.649e$ for **BDM** and $0.613e$ for **BDBM**, respectively. Meanwhile, the estimated differences between $\mu_e$ and $\mu_g$ are 13.2 Debye for **BDM** and 10.5 Debye for **BDBM** (Table S3†), which are sufficiently large to cause significant solvatochromism according to previous studies.[55] The calculated charge transfer and difference between the excited-state and ground-state dipole moments suggest a stronger ICT effect for **BDM** than that for **BDBM**, in accordance with the slopes of the
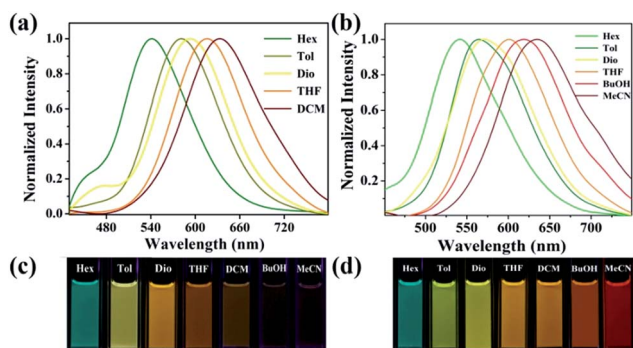


**Fig. 1** Normalized fluorescence spectra of (a) **BDM** and (b) **BDBM** in different solvents. Photographs of (c) **BDM** and (d) **BDBM** under UV illumination in different solvents. Hex, hexane; Tol, toluene; Dio, dioxane; THF, tetrahydrofuran; DCM, dichloromethane; BuOH, *n*-butanol; MeCN, acetonitrile. Concentration: 10 μmol L$^{-1}$; excitation wavelength: 400 nm.
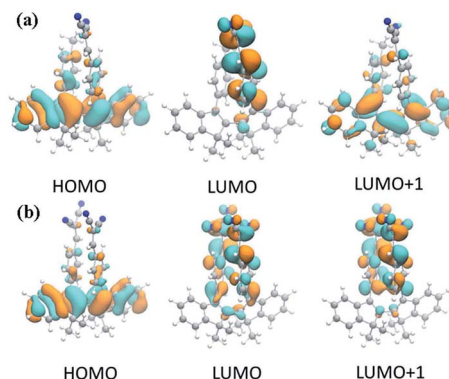


**Fig. 2** Frontier molecular orbitals of (a) **BDM** and (b) **BDBM**.

fitting lines in the $\Delta \nu$–$\Delta f$ plots (Fig. S2a†). TD-DFT calculations suggest that the oscillator strengths of the HOMO → LUMO and the transition in **BDM** is twice as large as that of **BDBM** (Table S2†); however, it is noteworthy that the second lowest excited state (S2) of **BDBM** is also of ICT character and exhibits a slightly larger excitation energy than the S1 state. The oscillator strength of the S0 → S2 excitation for **BDBM** is five-fold larger than that of S0 → S1 excitation for **BDBM** and two-fold larger than that of S0 → S1 excitation for **BDM**, explaining the experimentally observed higher extinction coefficient of **BDBM** at around 400 nm (Fig. S1†). TD-DFT calculations also predict that the S3 and S4 states of **BDBM** contribute to the absorption band at around 320 nm, while for **BDM** the S2 and S3 states make non-negligible contribution. The calculated oscillator strengths of these excited states agree with the higher extinction coefficient of **BDBM** in the ultra-violet region (Fig. S1†). Therefore, the absorption bands of both compounds at the longer wavelengths (∼400 nm) originate from ICT-type excitations, *e.g.* HOMO → LUMO transition of **BDM** and HOMO → LUMO and HOMO → LUMO + 1 transition of **BDBM**, while the absorption bands at the shorter wavelengths (∼320 nm) correspond to the local excitations of the biindene chromophore. It is also noteworthy that the second lowest excited state (S$_2$) of **BDBM**, which corresponds to HOMO → LUMO + 1 transition, is also of ICT character and exhibits a slightly larger excitation energy compared with the S$_1$ state. Differently, in **BDM** the LUMO + 1 orbital is located on the central indene rings and the S$_2$ state corresponding to HOMO → LUMO + 1 transition has a much larger excitation energy in the ultraviolet region.

### Detection of low-level water

Clearly, the fluorescence emissions of **BDM** and **BDBM** are highly sensitive to solvent polarity according to the above discussions. Therefore, we further investigated their emission behaviour in non-hydrogen-bond donating water-miscible solvents, *i.e.*, THF and dioxane. As shown in Fig. S4,† the absorption spectra of **BDM** and **BDBM** in THF solution underwent slight changes from pure THF to THF containing 10% (v/v) water, indicating that neither solvent polarity nor hydrogen bonding has a significant influence on the absorption spectra. In contrast, upon further addition of water in THF solution, the emission band of **BDM** was effectively quenched and that of **BDBM** was gradually diminished along with bathochromic shift from 597 nm to 617 nm (Fig. 3a–d). These phenomena can be attributed to the cooperative effect of the solvent polarity and the ICT.[56,57] Fig. S5a† shows in details how the measured fluorescent intensity changed as a function of water content in the THF solution of **BDM**. As can be seen from the graph, the fluorescent intensity of **BDM** decreased dramatically when the water content was below 4.00% (v/v): the reduction in relative fluorescence intensity reached nearly 57%, whereas such effect became moderate when the water content was higher than 4.00% (v/v). More importantly, the fluorescent intensity of **BDM** as a function of water content showed a good linear relationship below 1% (v/v), and the detection limit of **BDM** for water was determined as 0.010% (113 ppm) in THF (Fig. S5b†). In
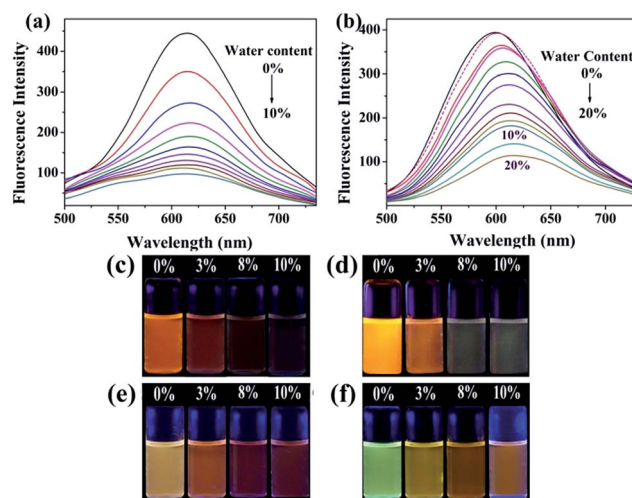


Fig. 3 Fluorescence spectra of (a) BDM and (b) BDBM in THF solution in the presence of increasing amount of water. The emission changes of (c) BDM and (d) BDBM in THF solution containing different amounts of water. The emission changes of (e) BDM and (f) BDBM in dioxane solution containing different amounts of water. Concentration: 10 μmol L$^{-1}$; excitation wavelength: 400 nm.

comparison with reported solvatochromic dyes for the detection of water in organic solvents,[26,56] the detection limit of **BDM** was moderate, demonstrating that **BDM** is sensitive to low-level water content in THF. Compared with **BDM**, the fluorescent intensity of **BDBM** as a function of water was a bit less sensitive, but it could also be used as an indicator of water (Fig. 3b).

Similar to THF, the emission spectra of **BDM** and **BDBM** in dioxane solution also underwent significant changes from pure dioxane to dioxane containing 10% (v/v) water. In comparison with THF, the emission maxima of both compounds in dioxane solution were more sensitive to water, which displayed relatively large red-shifts (**BDM**: 18 nm; **BDBM**: 33 nm) (Fig. S6a and b† and 3e and f). As shown in Fig. S5d,† the fluorescence peak of **BDM** also showed a good linear relationship below 1% (v/v), and the detection limit of **BDM** for water was 0.019% (212 ppm) in dioxane. Therefore, the distinct fluorescence responses of **BDM** and **BDBM** caused by water revealed that they can serve as suitable water indicators to detect low-level water content in THF or dioxane qualitatively. Particularly for **BDM**, it can be also utilized to quantitatively detect low-level water content in organic solvents.

### AIEE behaviours and efficient solid emitter

To investigate the AIEE properties of **BDM** and **BDBM**, we employed anhydrous DMSO as the good solvent and water as the poor solvent. The absorption and emission spectra of both compounds in DMSO and DMSO/water mixture solutions were recorded (Fig. 4 and S7†). Clearly, the fluorescent intensity of **BDBM** was rather weak in pure DMSO solution (Fig. 4b and d). However, the fluorescent intensity increased dramatically when the water content was above 40%. As the water content reached 70%, the photoluminescence intensity was boosted to the maximum. With the increase of the water content from 70% to
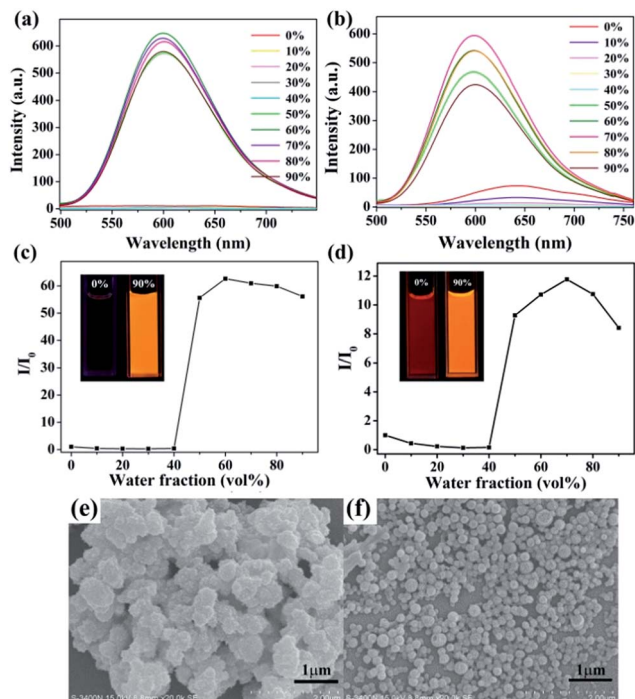
Fig. 4 Fluorescence spectra of BDM (a) and BDBM (b) in DMSO−water mixtures with different water contents. Plots of $I/I_0$ values *versus* water content of the solvent mixture for BDM (c) and BDBM (d). Inset: the corresponding fluorescence images under UV illumination. SEM images of BDBM nanoaggregates obtained from (e) 70% and (f) 90% DMSO−H$_2$O mixtures, respectively. Concentration: 10 μmol L$^{-1}$; excitation wavelength: 400 nm.

90%, the emission spectra of BDBM showed a decrease in the intensity. Eventually, the emission intensity of BDBM was approximately 8 folds higher than its molecularly dispersed species in DMSO. The apparent emission enhancement of BDBM was thus induced by aggregation, verifying its AIEE nature owing to the restricted intramolecular motions (RIM) mechanism:[58,59] large amount of water resulted in formation of aggregated nanoparticles, which subsequently impeded the intramolecular rotations of the aromatic rotors of BDBM and endowed the aggregates with intense emission. The nanoparticles from the aqueous mixtures were obtained by solvent evaporation. As shown in Fig. 4e and f, the nanoparticles formed in the 70% aqueous mixture were larger than those obtained from the 90% aqueous mixture. The decrease of the fluorescence intensity mentioned above was related to this result, which was probably ascribed to the change in the packing pattern of the dye molecules in the aggregates.[60] In the mixture with 70% water content, the dye molecules are expected to steadily assemble in an ordered fashion to form more emissive crystalline aggregates, while in the mixture with 90% water content, the dye molecules may quickly agglomerate in a random way to form less emissive amorphous particles.

Moreover, compared to the pure DMSO solution of BDBM, the emission maximum of the aggregates blue-shifted from 625 nm to 600 nm, and the emission colour changed from red to orange (Fig. 4d insert). The weak and redder emission in pure

DMSO solution implied the existence of large-amplitude relaxation in the excited state, such as intramolecular charge transfer (ICT).[61] Nevertheless, aggregation forced the molecules to reside in an apolar environment which is unfavourable for ICT process, resulting in the blue shift of the emission maximum and was also helpful for the light emission. In contrast to the fluorescence, the absorption spectra of BDBM was red-shifted and broadened upon addition of water, due to the nano-aggregated structure of the molecules (Fig. S7b†). Meanwhile, the level-off tails in the visible region of the absorption spectra clearly indicated the formation of aggregates. The scanning electron microscopy (SEM) images also displayed the formation of well-defined nanoparticles in aqueous mixtures (Fig. 4f).

A similar phenomenon was observed for BDM. The pure DMSO solution of BDM was almost nonemissive and the fluorescence spectra was almost parallel to the abscissa. However, BDM exhibited a strong luminescence with a 56-fold increase in the $I/I_0$ ratio when the water concentration reached 90% (Fig. 4a and c), demonstrating that BDM possessed the typical characters of AIEE. Besides, the emission maximum of the aggregates of BDM blue-shifted from 628 nm to 600 nm, and the emission colour changed from red to orange.

The AIEE feature was also confirmed by the intense fluorescent images of the solid (Fig. 5). The solid was recrystallized from acetone and the emission colours of BDM and BDBM were bright yellowish orange and orange, respectively. To evaluate the AIEE effect, the emission spectra and fluorescence quantum yield of the two compounds were measured. Both BDM and BDBM exhibited intense emission peaking at 626 nm and 635 nm, respectively. In contrast to the low quantum yields of <1% and 1% in DMSO solution (Table S1†), the solid state fluorescent quantum yields of BDM and BDBM were determined as 24% and 22%, respectively. Such high $\Phi_F$ values endorse their great prospects in OLED applications.[62]

The single crystal of BDBM was obtained for further verification of the mechanism of the AIEE system. As shown in Fig. 6a, the interplane angle ($\theta_1$) between the two indene aromatic rings was 48.2°, which indicated that the core
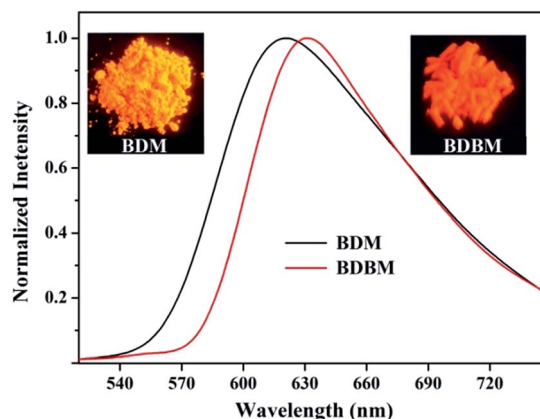


Fig. 5 Normalized fluorescence spectra of the two solids. Inset: the corresponding fluorescence images of BDM and BDBM under illumination. Excitation wavelength: 400 nm.
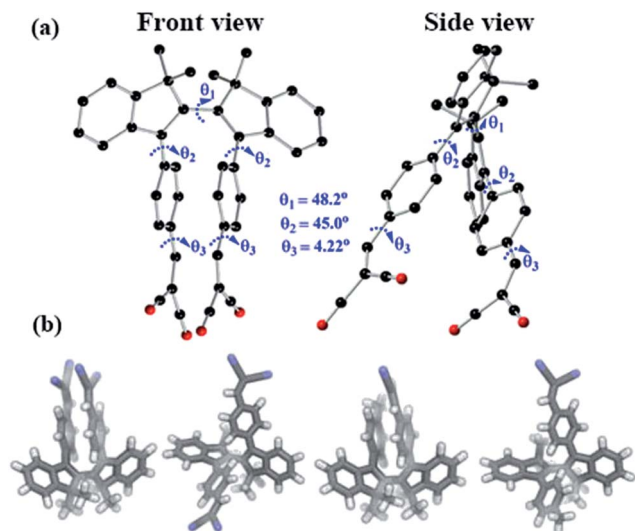
Fig. 6 (a) Single-crystal structure of compound **BDBM**. (b) Optimized geometries. From left to right: **BDBM-s** (stacked), **BDBM-t** (twisted), **BDM-s** (stacked), **BDM-t** (twisted).

structure of 2,2′-biindene was nonplanar. Furthermore, the indene planes and the aryl substituents were not coplanar either, where the dihedral angles ($\theta_2$) were 45.0°. Owing to the twisted structure, the conformation of **BDBM** strongly deviated from a planar conformation and prevented the rings from undergoing π–π stacking interactions, thus inducing intense emission in the condensed state. Another notable feature of **BDBM** was that the terminal dicyanovinyl groups were almost coplanar with the attached benzene ring (dihedral angle $\theta_3 =$ 4.22°), suggesting the effective conjugation between the dicyanovinyl groups and the 2,2′-biindene main chain framework.

To gain insight into the structure–property relationship of compounds **BDM** and **BDBM**, we employed density functional (DFT) calculations to optimize their geometries, as shown in Fig. 6b. Each compound has two possible conformations, namely the stacked and the twisted conformation of the two phenyl rings. Our calculations suggest that the stacked conformation is more stable than the twisted conformation by around 7 kJ mol⁻¹ (Table S4†), in consistency with experimentally observed crystal structure. In fact, the dispersion interaction plays an important role in stabilizing the π–π stacked conformations, which offers a stabilization energy of 29 kJ mol⁻¹ for **BDBM** and 19 kJ mol⁻¹ for **BDM**, respectively. We also measured the dihedral angles between different panels as shown in Fig. S8.† The dihedral angles between the two five-membered rings are around 44° in both compounds, while the dihedral angles between the central unit and peripheral phenyl rings range from 46° to 49°, in which $\theta_3$ of **BDM** is the smallest, most likely owing to the relatively weak steric effect of the methyl group. The calculated dihedral angles for **BDBM** are close to the corresponding dihedral angles in single-crystal structure (43.6°/48.2°, 48.5°/45.0°). These calculations demonstrate the nonplanar structures of two compounds, in agreement with their AIEE properties.

### Detection of cyanide

Recently, the dicyanovinyl group as the reactive unit has been widely employed to construct reaction-based cyanide sensors.[63,64] Thus **BDM** and **BDBM** may have great potential for detection of cyanide in aqueous media based on their AIEE properties. The sensor systems were prepared by mixing the AIEE dyes in DMSO (50 μL, 2.0 mmol L⁻¹) and CTAB in water (5 mL, 2.0 mmol L⁻¹).[49] Both two compounds were readily dispersed in water and the mixture solution emitted intense fluorescence. The quenching of fluorescence was attributed to two main aspects: (i) the nucleophilic addition of cyanide to the dicyanovinyl group of **BDM** and **BDBM** led to the formation of water-soluble compounds with negative charges, resulting in disassembly of the nanoparticles and decrease of the emission;[26] (ii) the nucleophilic attack of cyanide to the dicyanovinyl group of the two compounds would interrupt the π-conjugation and disrupt the ICT transition, leading to significant decrease in fluorescence.[46] It is certain that the ICT transition reduction is the reason for fluorescence quenching, because the absorbance at excited wavelength markedly decreased after CN⁻ addition.

Compound **BDBM** was utilized to investigate in detail the interaction of both compounds with cyanide through absorption and fluorescence spectra titration experiments. Probe **BDBM** was light yellow and exhibited main absorption bands centred at 333 and 408 nm, respectively (Fig. 7a). Upon addition of 0–9.0 equiv. of cyanide, both bands gradually decreased and
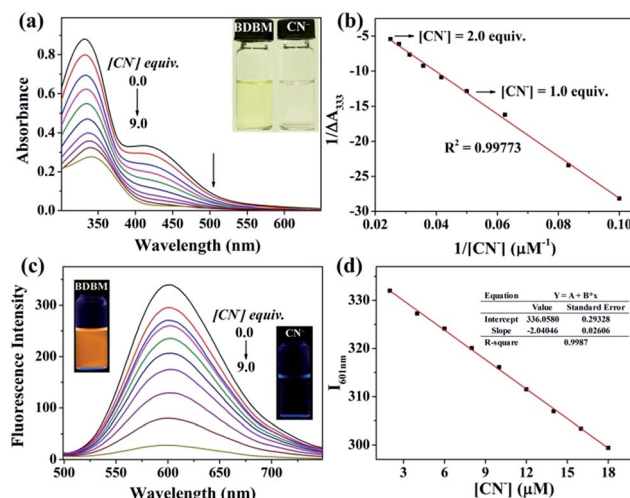


Fig. 7 (a) Absorption spectral changes of **BDBM** (20 μmol L⁻¹) upon addition of 0–9.0 equiv. of cyanide in 2 mmol L⁻¹ CTAB micellar solution. Insert: the images of **BDBM** with different amount of cyanide (left: none; right: 9.0 equiv. cyanide). (b) Benesi–Hildebrand plot of absorbance at 333 nm. (c) Fluorescence spectra of **BDBM** (20 μmol L⁻¹) upon addition of 0–9.0 equiv. of cyanide in 2 mmol L⁻¹ CTAB micellar solution. Insert: the images of fluorescence with different amount of cyanide (left: none; right: 9.0 equiv. of cyanide). (d) Plot of fluorescence intensity *versus* cyanide concentration, $\lambda_{ex} = 400$ nm, $\lambda_{em} = 601$ nm, $R^2 = 0.9987$, $k = 2.04$ μM⁻¹, $\sigma = 0.20$. The standard deviation ($\sigma$) was obtained by fluorescence responses (10-times of consecutive scanning on the Varian Cary Eclipse Fluorescence Spectrophotometer). The detection limit was calculated as 0.29 μM by the formula ($3\sigma/|k|$).

the one at 408 nm eventually vanished at the saturation point (9.0 equiv.). This change suggests that the large π-conjugation was interrupted, accompanied by the formation of [CN–BDBM–CN]$^{2-}$ due to the nucleophilic attack of cyanide toward the dicyanovinyl groups of **BDBM**. The Benesi–Hildebrand plot of absorbance at 333 nm upon addition of cyanide is shown in Fig. 7b. The linear correlation between $1/\Delta A_{333}$ and $1/[CN^-]$ implied the 1 : 1 stoichiometric reaction between **BDBM** and cyanide. Moreover, the solvent faded and became almost colourless, which could be clearly observed by naked eye (Fig. 7a inset).

As expected, the fluorescence emission of **BDBM** was quenched by the nucleophilic addition reaction between cyanide and dicyanovinyl group. Upon excitation at 400 nm, a broadened emission band at around 601 nm was detected, which gradually decreased upon addition of cyanide and became saturated with 9.0 equiv. of CN$^-$ (Fig. 7c). Additionally, a linear relationship between the fluorescent intensity at 601 nm and the concentration of CN$^-$ in the low concentration region was obtained (Fig. 7d). The detection limit was as low as 0.29 μM, which amounts to one sixth of the maximum contaminant level (MCL) for CN$^-$ in drinking water (1.9 μM) set by the World Health Organization (WHO). In comparison with reported probes,[26,35,37] the detection limits of **BDBM** is one of the lowest fluorescence detection limits to cyanide in water. The prompt response of **BDBM** to cyanide in CTAB micelles was attributed to the electrostatic interactions between anionic cyanide and cationic CTAB, which would attract the cyanide to the micellar surface and thus facilitate the attack of cyanide to **BDBM**.[65,66] Moreover, CTAB provided a hydrophobic environment which could effectively eliminate the negative effect of water on specific cyanide reaction. These results indicate that **BDBM** possesses a high sensitivity toward cyanide in nearly pure water surroundings, endorsing its practical application for detecting cyanide.

Similar to probe **BDBM**, the absorption spectra of probe **BDM** showed two absorption bands centred at 326 and 398 nm, respectively (Fig. S9a†). Upon addition of 0–7.0 equiv. of cyanide, both absorption bands gradually decreased and the band at 408 nm finally disappeared. The linear correlation between $1/\Delta A_{326}$ and $1/[CN^-]$ confirmed the 1 : 1 stoichiometric reaction between **BDM** and CN$^-$ with formation of [**BDM–CN**]$^-$ (Fig. S9b†). Accordingly, the solution of probe **BDM** changed from light yellow to colourless upon addition of CN$^-$, which can be detected by naked eye (Fig. S9a† inset). Furthermore, upon excitation at 400 nm, a broadened emission band at around 603 nm was detected, which gradually reduced with the addition of cyanide and vanished with 7.0 equiv. of CN$^-$ (Fig. S9c†). The detection limit of probe **BDM** for cyanide was obtained using a fluorescence intensity plot against CN$^-$ concentration ranging from 0.4 to 1.1 equiv. (Fig. S9d†), which provided a good linear correlation and an outstanding detection limit of 0.32 μM.

To investigate the reaction processes of the probes, we monitored the $^1$H NMR spectral changes of probe **BDM** and **BDBM** in DMSO-$d_6$ upon addition of 0–1.0 and 0–2.0 equiv. of cyanide in CH$_2$Cl$_2$, respectively. In the case of **BDBM** (Fig. 8), the two vinylic protons (Ha) at 8.41 ppm gradually decreased and

eventually disappeared upon addition of 2.0 equiv. of cyanide. Concurrently, two new signals appeared at 4.52, 4.48 ppm (Hb, Hb′), respectively. The upfield shift of aromatic proton signal was induced by the broken conjugation between the dicyanovinyl groups and the 2,2′-biindene framework, which was caused by the nucleophilic addition of cyanide to the dicyanovinyl groups. Furthermore, no signal corresponding to the malononitrile moiety (Ha) was observed in the $^1$H NMR spectra, implying the formation of a stabilized anionic species in the medium.[41] The formed anionic adduct **BDBM–CN** was dissolved in water, destructing the aggregated nanoparticles and quenching the emission. The $^1$H NMR titration of **BDM** by CN$^-$ presented a similar pattern to that of **BDBM** (Fig. S10†). Upon the addition of 1.0 equiv. of cyanide anion, the vinylic proton (Ha) at 8.46 ppm gradually vanished. Meanwhile, a new signal appeared at 4.51 ppm (Hb), indicating that the cyanide reacted with the dicyanovinyl groups. It was further confirmed by MS (ESI) experiments (Fig. S11 and S12†).

In addition, the rapid detection of cyanide in aqueous media is one of the most important factors for practical applications. In order to estimate the response rates of **BDM** and **BDBM** to cyanide, time-dependent fluorescence intensity changes with the addition of different concentrations of CN$^-$ were measured (Fig. 9). It is noteworthy that the fluorescence of **BDM** and **BDBM** were quenched almost completely in less than 100 seconds upon addition of 7.0 equiv. and 9.0 equiv. of CN$^-$, respectively. The fast response was attributed to two main aspects: (i) the electrostatic interaction between anionic cyanide and cationic CTAB accelerated the rapid attack of cyanide to the dicyanovinyl groups of two compounds; and (ii) the formation of the uniform and smaller nanoparticles of **BDM** and **BDBM**
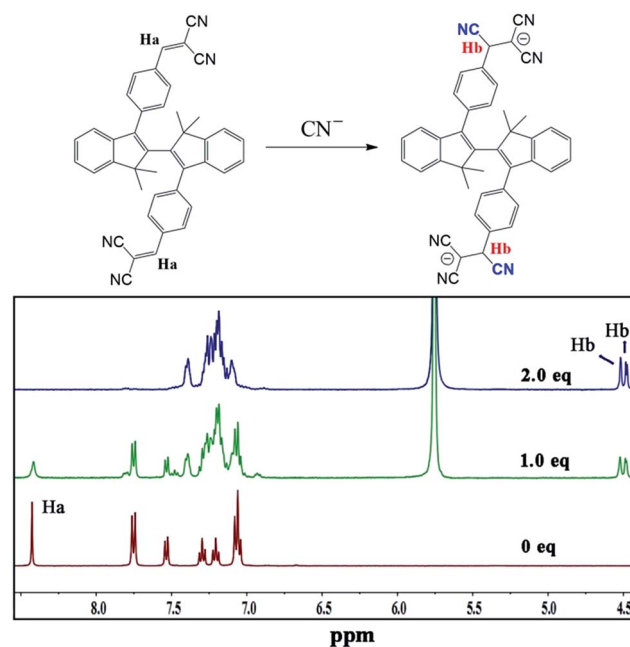


**Fig. 8** $^1$H NMR spectra of **BDBM** in DMSO-$d_6$ upon addition of cyanide in CH$_2$Cl$_2$.
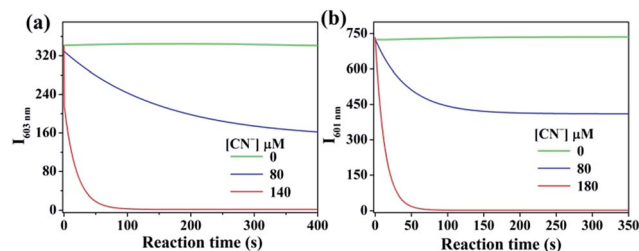
**Fig. 9** Time-dependent changes of (a) **BDM** and (b) **BDBM** in the fluorescence intensity with different amounts of cyanide. Concentration: 20 µmol L$^{-1}$; excitation wavelength: 400 nm.



**Fig. 11** Frontier molecular orbitals of [CN–BDBM–CN]$^{2-}$.

molecules assisted by CTAB contributed to the short detection process.[26,49,67]

Furthermore, high selectivity and anti-interference ability are important features for chemodosimeters. To evaluate the selectivity of the two probes for cyanide detection, the changes of **BDM** and **BDBM** in absorption and fluorescence spectra caused by CN$^-$ (7.0 equiv., 9.0 equiv.) and miscellaneous interference anions (F$^-$, Cl$^-$, Br$^-$, I, H$_2$PO$_4^-$, AcO$^-$, HCO$_3^-$, NO$_3^-$, NO$_2^-$, 45 equiv.) were recorded. As shown in Fig. 10a–d and S13,† the addition of CN$^-$ produced remarkable changes in both absorption and fluorescence spectra, with the solution colour changing from light yellow to colourless and the emission colour from intense orange to colourless. Nevertheless,
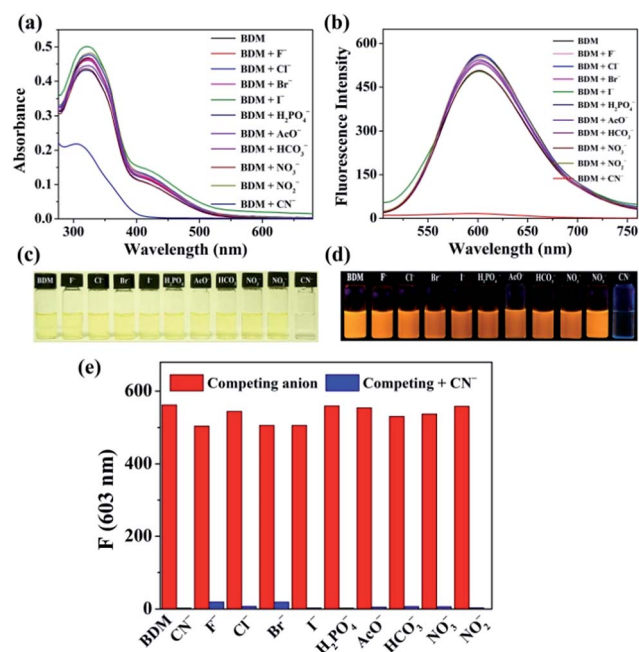


**Fig. 10** (a) Absorption spectra and (b) fluorescence of **BDM** in CTAB micelles (2 mmol L$^{-1}$) upon addition of various anions (CN$^-$: 7.0 equiv., other anions: 45.0 equiv.). The corresponding colour (c) and emission (d) changes of **BDM** in CTAB micelles (2 mmol L$^{-1}$) upon addition of various anions. Concentration: 20 µM; excitation wavelength: 400 nm. (e) The fluorescence intensity changes at 603 nm of **BDM** (20 mM) upon addition of 7.0 equiv. of CN$^-$ and 45.0 equiv. of various interference anions.
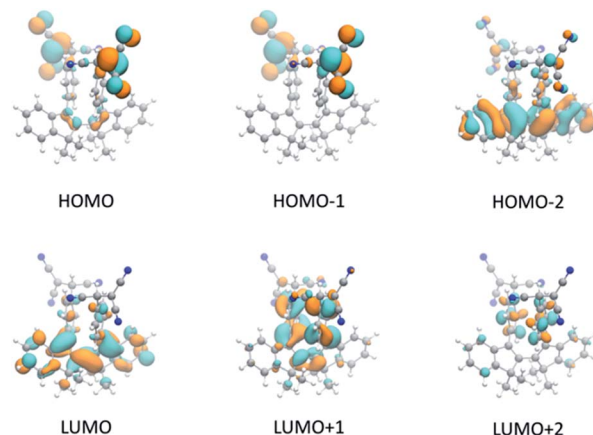
there was no significant change in spectra, solution colour and emission colour when other anions were added. These results demonstrated the high sensing selectivity of **BDM** and **BDBM** toward cyanide over other anions in nearly pure water surroundings. More importantly, the competitive experiments further confirmed that both probes could selectively detect cyanide even in the presence of higher concentration of the above-tested anions (Fig. 10e and S14†). The excellent selectivity of two compounds in water was ascribed to the specific nucleophilic addition of cyanide to the dicyanovinyl group, strengthening their great potentials in practical applications.

To gain further insight into the cyanide-sensing process of **BDM** and **BDBM**, DFT calculations were carried out. Upon addition of cyanide, the dicyanovinyl groups are subject to nucleophilic reaction, forming the adducts [CN–BDBM–CN]$^{2-}$ and [CN–BDM]$^-$, whose optimized geometries are shown in Fig. S15.† The electronic structures of the two compounds are in turn significantly altered. As shown in Fig. 11, the HOMO and HOMO − 1 of [CN–BDBM–CN]$^{2-}$ are both located at the anionic part, while HOMO − 2 receives contributions mainly from the central indene rings. The lowest excited state of [CN–BDBM–CN]$^{2-}$ corresponds to the HOMO − 2 → LUMO transition, which is the local excitation of the indene units. Similarly, the HOMO of [CN–BDM]$^-$ is located at the anionic part, and the HOMO − 1 receives its main contribution from the central indene units (Fig. S16†). The lowest excited state of [CN–BDM]$^-$ corresponds to the HOMO − 1 → LUMO transition, namely the local excitation of the indene units. The ICT effects in [CN–BDBM–CN]$^{2-}$ and [CN–BDM]$^-$ thus vanished due to nucleophilic attack of the cyanide anions, and the maximum absorption wavelengths of both adducts are reduced to around 350 nm (Table S5†). The fluorescence at around 600 nm thus disappeared, in agreement with experimental observations.

## Conclusions

Novel biindenyl-based D–π–A derivatives, **BDM** and **BDBM**, containing electron-withdrawing dicyanovinyl groups have been successfully developed. Both compounds display intense

ICT fluorescence in different solvents and exhibit highly efficient emission in the solid state. Moreover, they could be utilized as fluorescent sensors for the qualitative detection of low-level water content in THF or dioxane. In particular, the low detection limit of **BDM** (113 ppm in THF) enables it a supersensitive water sensor for practical applications. Furthermore, both compounds show prompt responses to cyanide under the assistance of CTAB, thus giving two sensitive chemo-sensors with highly selectivity and low detection limits. In particular, a remarkable detection limit of 0.29 μmol L$^{-1}$ as well as a short response time of only 100 seconds to cyanide was obtained for **BDBM** in aqueous media, promising its practical applications for detecting cyanide in drinking water. Notably, our results not only provide a successful example of the ratiometric fluorescent sensor for water in organic solvent and cyanide in aqueous media, but also demonstrate practical applications of our π-conjugated molecules. We envisage that the molecular design concept and the practical applications presented in this work can promote future research in the field and enable further development of novel bio/chemosensors with intriguing optoelectronic properties and outstanding performance.

# Experimental section

## Materials

Compounds **1** and **3** were synthesized according to previous method.[12] Other reactants were purchased commercially, and used as received without further purification. Dioxane and THF were pre-dried over 4 Å molecular sieves and distilled under nitrogen atmosphere from sodium and benzophenone immediately prior to use. Other solvents were dried with 4 Å molecular sieves prior to use. Double distilled water from a Millipore Milli-Q plus system was used throughout the work. Cyanide anion was in the form of tetrabutylammonium (TBA) salts, solutions of other anions were prepared from the corresponding sodium salts.

## Instrumentation

$^1$H NMR and $^{13}$C NMR spectra were recorded on Brucker AM-400 spectrometers. Chemical shifts were reported in ppm relative to a tetramethylsilane (TMS) standard in CDCl$_3$ or DMSO-$d_6$. Mass spectra (MS) were obtained on a Waters LCT Premier XE spectrometer. UV-vis absorption spectra were performed on a Varian Cray 500 spectrophotometer and fluorescence spectra were recorded on a Varian Cray Eclipse. Quantum yields of samples were recorded on a Horiba Fluoromax-4 with a calibrated integrating sphere system. The melting points were measured on an X4 Micro-melting point apparatus.

## Evaluation of solvatochromism

The effects of solvents on the emission features can be evaluated by the relationship between the solvent polarity parameter ($\Delta f$) and Stokes shift ($\Delta \nu$) of the absorption and emission maxima (Lippert–Mataga equation).

$$\Delta \nu \equiv \nu_{ab} - \nu_{em} = \frac{2\Delta f}{hc\alpha^3}(\mu_e - \mu_g)^2 + \text{const} \qquad (1)$$

where $\Delta \nu$ is the Stokes shift, $\Delta f$ is the solvent orientation polarizability, $h$ is the Planck constant, $c$ is the speed of light in vacuum, $\alpha$ is the Onsager cavity radius, $\mu_e$ and $\mu_g$ are the dipole moments in the excited (e) and ground (g) states, respectively.

## Computational method

We employed density functional theory (DFT) calculations to optimize the geometries of compounds **BDBM** and **BDM**, using the hybrid B3LYP functional[68] and the double-zeta basis set 6-31G(d,p).[69] Grimme's dispersion correction (version D3)[70] was employed in DFT calculations. At the optimized geometries, frequency analyses were performed to confirm that these geometries are true minima on the potential energy surface. Time-dependent (TD) DFT calculations were also carried out to provide insight into molecular orbital compositions of the excited singlet states, using the range-separated CAM-B3LYP functional[71] and the triple-zeta basis set 6-311+G(2d,p)[72] where diffuse functions are included. Solvent effects of CH$_2$Cl$_2$ were taken into account by the polarizable continuum model (PCM)[73] in TD-DFT calculations. All calculations were carried out using the Gaussian09 program package.[74]

## Synthesis

**4-(1,1,1′,1′-Tetramethyl-3′-(p-tolyl)-1H,1′H-[2,2′-biinden]-3-yl)-benzaldehyde (2).** A solution of **1** (5.00 g, 10.7 mmol), N-bromosuccinimide (NBS) (2.30 g, 12.8 mmol) and azodiisobutyronitrile (AIBN) (0.08 g, 0.5 mmol) in carbon tetrachloride (100 mL) was heated for 10 h under reflux. The reaction mixture was cool to room temperature and rotary evaporated to a residue. The residue was heated in ethanol (20 mL) for 1 h under reflux, and then cool to room temperature, and followed by vacuum filtration gave a yellow solid. The solid was heated in DMSO (30 mL) in 150 °C until no hydrogen bromide gas released. After cooling to room temperature, the solution was poured into the distilled water (100 mL) to precipitate the product. Then the precipitate was filtered and purified by silica gel column chromatography using petroleum ether–CH$_2$Cl$_2$ as eluent. A yellow-green solid was obtained (yield: 0.95 g, 18%). $^1$H NMR (400 MHz, DMSO-$d_6$, δ): 9.96 (s, 1H), 7.80 (d, 2H, J = 8.2 Hz), 7.43 (dd, 2H, $J_1$ = 10.8 Hz, $J_2$ = 7.0 Hz), 7.33 (d, 2H, J = 8.1 Hz), 7.28–7.15 (m, 4H), 7.08 (dd, 4H, $J_1$ = 9.0 Hz, $J_2$ = 6.1 Hz), 7.00 (d, 2H, J = 8.1 Hz), 2.28 (s, 3H), 1.51 (d, 6H, J = 5.3 Hz), 1.10 (d, 6H, $J_1$ = 11.3 Hz). $^{13}$C NMR (100 MHz, CDCl$_3$, δ): 192.02, 154.81, 154.73, 149.92, 146.31, 143.16, 142.92, 141.72, 141.26, 141.11, 136.69, 134.65, 133.03, 129.63, 128.98, 128.74, 126.38, 126.34, 125.90, 125.80, 121.13, 120.93, 120.89, 120.36, 53.44, 53.14, 28.54, 28.44, 24.67, 24.49, 21.20. HRMS (ESI, m/z): [M + H]$^+$ calcd for C$_{36}$H$_{33}$O, 481.2531; found, 481.2525.

**2-(4-(1,1,1′,1′-Tetramethyl-3′-(p-tolyl)-1H,1′H-[2,2′-biinden]-3-yl)benzylidene)malononitrile (BDM).** The mixture of excess malononitrile, ammonium acetate (0.08 g, 1.0 mmol) and **2** (0.50 g, 1.0 mmol) was dissolved in acetic acid (50 mL) and refluxed under an nitrogen atmosphere for 6 h. After cooling to room temperature, the mixture was poured into water, and the precipitation was purified by silica gel chromatography using petroleum ether–CH$_2$Cl$_2$ as eluent. A deep yellow solid was

obtained (yield: 0.30 g, 55%). $^{1}$H NMR (400 MHz, DMSO-$d_6$, $\delta$): 8.46 (s, 1H), 7.82 (d, 2H, $J = 8.4$ Hz), 7.46 (t, 2H, $J = 7.6$ Hz), 7.28–7.17 (m, 6H), 7.11–7.03 (m, 4H), 6.92 (d, 2H, $J = 8.1$ Hz), 2.28 (s, 3H), 1.56 (d, 6H, $J = 4.6$ Hz), 1.20 (d, 6H, $J = 1.7$ Hz). $^{13}$C NMR (100 MHz, CDCl$_3$, $\delta$): 158.25, 153.93, 153.84, 149.88, 145.07, 142.70, 142.40, 140.49, 189.96, 139.60, 135.80, 131.77, 129.72, 129.01, 128.09, 128.03, 127.58, 125.45, 125.39, 125.11, 125.00, 120.24, 120.02, 119.93, 119.21, 112.98, 111.81, 80.52, 52.28, 51.90, 27.67, 27.50, 23.46, 23.23, 20.14. HRMS (ESI, $m/z$): [M + NH$_4$]$^{+}$ calcd for C$_{39}$H$_{36}$N$_3$, 546.2909; found, 546.2912.

**2,2′-(((1,1,1′,1′-Tetramethyl-1$H$,1′$H$-[2,2′-biindene]-3,3′-diyl)-bis-(4,1-phenylene))-bis-(methanylylidene))dimalononitrile (BDBM).** The mixture of excess malononitrile, ammonium acetate (0.16 g, 2.1 mmol) and **2** (0.50 g, 1.0 mmol) was dissolved in acetic acid (50 mL) and refluxed under an nitrogen atmosphere for 6 h. After cooling to room temperature, the mixture was poured into water, and the precipitation was purified by silica gel chromatography using petroleum ether–CH$_2$Cl$_2$ as eluent. A orange solid was obtained (yield: 0.45 g, 75%). $^{1}$H NMR (400 MHz, DMSO-$d_6$, $\delta$): 8.41 (s, 2H), 7.74 (d, 4H, $J = 8.3$ Hz), 7.53 (d, 2H, $J = 7.4$ Hz), 7.29 (t, 2H, $J = 7.4$ Hz), 7.20 (t, 2H, $J = 7.4$ Hz), 7.05 (m, 6H), 1.64 (s, 6H), 1.40 (s, 6H). $^{13}$C NMR (100 MHz, CDCl$_3$, $\delta$): 159.13, 155.12, 149.76, 142.83, 142.41, 139.95, 130.79, 129.74, 129.35, 126.85, 126.77, 121.44, 120.58, 113.74, 112.86, 82.38, 52.97, 28.87, 23.88. HRMS (ESI, $m/z$): [M + H]$^{+}$ calcd for C$_{42}$H$_{31}$N$_4$, 591.2549; found, 591.2540.

## Acknowledgements

## Notes and references

1 J. Luo, Z. Xie, J. W. Y. Lam, L. Cheng, H. Chen, C. Qiu, H. S. Kwok, X. Zhan, Y. Liu, D. Zhu and B. Z. Tang, *Chem. Commun.*, 2001, 1740.

2 B. K. An, S. K. Kwon, S. D. Jung and S. Y. Park, *J. Am. Chem. Soc.*, 2002, **124**, 14410.

3 J. Huang, R. Tang, T. Zhang, Q. Li, G. Yu, S. Xie, Y. Liu, S. Ye, J. Qin and Z. Li, *Chem.–Eur. J.*, 2014, **20**, 5317.

4 J. Huang, N. Sun, P. Chen, R. Tang, Q. Li, D. Ma and Z. Li, *Chem. Commun.*, 2014, **50**, 2136.

5 X. Yao, X. Ma and H. Tian, *J. Mater. Chem. C*, 2014, **2**, 5155.

6 B. Sun, X. Yang, L. Ma, C. Niu, F. Wang, N. Na, J. Wen and J. Ouyang, *Langmuir*, 2013, **29**, 1956.

7 Z. Song, R. T. K. Kwok, E. Zhao, Z. He, Y. Hong, J. W. Y. Lam, B. Liu and B. Z. Tang, *ACS Appl. Mater. Interfaces*, 2014, **6**, 17245.

8 C. Zhang, S. Jin, S. Li, X. Xue, J. Liu, Y. Huang, Y. Jiang, W. Q. Chen, G. Zou and X. J. Liang, *ACS Appl. Mater. Interfaces*, 2014, **6**, 5212.

9 D. Li, J. Yu and R. Xu, *Chem. Commun.*, 2011, **47**, 11077.

10 W. Huang, F. Tang, B. Li, J. Su and H. Tian, *J. Mater. Chem. C*, 2014, **2**, 1141.

11 W. Huang, H. Wang, L. Sun, B. Li, J. Su and H. Tian, *J. Mater. Chem. C*, 2014, **2**, 6843.

12 Z. Zhang, B. Xu, J. Su, L. Shen, Y. Xie and H. Tian, *Angew. Chem., Int. Ed.*, 2011, **50**, 11654.

13 M. M. F. Choi and O. Ling Tse, *Anal. Chim. Acta*, 1999, **378**, 127.

14 A. Fong and G. M. Hieftje, *Anal. Chem.*, 1995, **67**, 1139.

15 A. Hakonen, *Anal. Chem.*, 2009, **81**, 4555.

16 Q. Chang, Z. Murtaza, J. R. Lakowicz and G. Rao, *Anal. Chim. Acta*, 1997, **350**, 97.

17 A. Hakonen and N. Stromberg, *Chem. Commun.*, 2011, **47**, 3433.

18 S. Ishihara, J. Labuta, T. Sikorsky, J. V. Burda, N. Okamoto, H. Abe, K. Ariga and J. P. Hill, *Chem. Commun.*, 2012, **48**, 3933.

19 Y. Ooyama, A. Matsugasako, Y. Hagiwara, J. Ohshita and Y. Harima, *RSC Adv.*, 2012, **2**, 7666.

20 B. P. Johnson, B. Gabrielsen, M. Matulenko, J. G. Dorsey and C. Reichardt, *Anal. Lett.*, 1986, **19**, 939.

21 H. Langhals, *Anal. Lett.*, 1990, **23**, 2243.

22 M. F. Vitha, *J. Chem. Educ.*, 2001, **78**, 370.

23 J. Jiang, X. Wang, W. Zhou, H. Gao and J. Wu, *Phys. Chem. Chem. Phys.*, 2002, **4**, 4489.

24 Z. Xu, X. Chen, H. N. Kim and J. Yoon, *Chem. Soc. Rev.*, 2010, **39**, 127.

25 X. Lou, D. Ou, Q. Li and Z. Li, *Chem. Commun.*, 2012, **48**, 8462.

26 Y. Zhang, D. Li, Y. Li and J. Yu, *Chem. Sci.*, 2014, **5**, 2710.

27 *Guidelines for Drinking-Water Quality*, World Health Organization, Geneva, Switzerland, 1996.

28 I. G. Casella and M. Gatta, *Electroanalysis*, 2001, **13**, 549.

29 Y. Yang, Q. Zhao, W. Feng and F. Li, *Chem. Rev.*, 2012, **113**, 192.

30 L. Yao, J. Zhou, J. Liu, W. Feng and F. Li, *Adv. Funct. Mater.*, 2012, **22**, 2667.

31 R. Gotor, A. M. Costero, S. Gil, M. Parra, R. Martinez-Manez, F. Sancenon and P. Gavina, *Chem. Commun.*, 2013, **49**, 5669.

32 S. Kumar, P. Singh, G. Hundal, M. Singh Hundal and S. Kumar, *Chem. Commun.*, 2013, **49**, 2667.

33 B. Chen, Y. Ding, X. Li, W. Zhu, J. P. Hill, K. Ariga and Y. Xie, *Chem. Commun.*, 2013, **49**, 10136.

34 X. Huang, X. Gu, G. Zhang and D. Zhang, *Chem. Commun.*, 2012, **48**, 12195.

35 B. Shi, P. Zhang, T. Wei, H. Yao, Q. Lin and Y. Zhang, *Chem. Commun.*, 2013, **49**, 7812.

36 C. Männel-Croisé, B. Probst and F. Zelder, *Anal. Chem.*, 2009, **81**, 9493.

37 L. G. Nandi, C. R. Nicoleti, I. C. Bellettini and V. G. Machado, *Anal. Chem.*, 2014, **86**, 4653.

38 F. Zelder and L. Tivana, *Org. Biomol. Chem.*, 2015, **13**, 14.

39 C. R. Nicoleti, L. G. Nandi and V. G. Machado, *Anal. Chem.*, 2015, **87**, 362.

40 X. Y. Shen, Y. J. Wang, E. Zhao, W. Z. Yuan, Y. Liu, P. Lu, A. Qin, Y. Ma, J. Z. Sun and B. Z. Tang, *J. Phys. Chem. C*, 2013, **117**, 7334.

41 S. J. Hong, J. Yoo, S. H. Kim, J. S. Kim, J. Yoon and C. H. Lee, *Chem. Commun.*, 2009, 189.

42 Z. Liu, X. Wang, Z. Yang and W. He, *J. Org. Chem.*, 2011, **76**, 10286.

43 X. Cheng, Y. Zhou, J. Qin and Z. Li, *ACS Appl. Mater. Interfaces*, 2012, **4**, 2133.

44 X. Cheng, R. Tang, H. Jia, J. Feng, J. Qin and Z. Li, *ACS Appl. Mater. Interfaces*, 2012, **4**, 4387.

45 Y. D. Lin, Y. S. Peng, W. Su, C. H. Tu, C. H. Sun and T. J. Chow, *Tetrahedron*, 2012, **68**, 2523.

46 L. Yang, X. Li, J. Yang, Y. Qu and J. Hua, *ACS Appl. Mater. Interfaces*, 2013, **5**, 1317.

47 G. L. Fu and C. H. Zhao, *Tetrahedron*, 2013, **69**, 1700.

48 C. Reichardt, *Chem. Rev.*, 1994, **94**, 2319.

49 R. Hu, J. Feng, D. Hu, S. Wang, S. Li, Y. Li and G. Yang, *Angew. Chem., Int. Ed.*, 2010, **49**, 4915.

50 C. Reichardt and T. Welton, *Solvents and Solvent Effects in Organic Chemistry*, Wiley-VCH Verlag GmbH & Co. KGaA, 2010, pp. 359–508.

51 P. Xue, B. Yao, J. Sun, Q. Xu, P. Chen, Z. Zhang and R. Lu, *J. Mater. Chem. C*, 2014, **2**, 3942.

52 J. S. Yang, K. L. Liau, C. M. Wang and C. Y. Hwang, *J. Am. Chem. Soc.*, 2004, **126**, 12325.

53 N. Mataga, Y. Kaifu and M. Koizumi, *Bull. Chem. Soc. Jpn.*, 1956, **29**, 465.

54 W. Z. Yuan, Y. Gong, S. Chen, X. Y. Shen, J. W. Y. Lam, P. Lu, Y. Lu, Z. Wang, R. Hu, N. Xie, H. S. Kwok, Y. Zhang, J. Z. Sun and B. Z. Tang, *Chem. Mater.*, 2012, **24**, 1518.

55 P. Pasman, F. Rob and J. W. Verhoeven, *J. Am. Chem. Soc.*, 1982, **104**, 5127.

56 L. Ding, Z. Zhang, X. Li and J. Su, *Chem. Commun.*, 2013, **49**, 7319.

57 R. Hu, E. Lager, A. Aguilar-Aguilar, J. Liu, J. W. Y. Lam, H. H. Y. Sung, I. D. Williams, Y. Zhong, K. S. Wong, E. Peña-Cabrera and B. Z. Tang, *J. Phys. Chem. C*, 2009, **113**, 15845.

58 J. Chen, C. C. W. Law, J. W. Y. Lam, Y. Dong, S. M. F. Lo, I. D. Williams, D. Zhu and B. Z. Tang, *Chem. Mater.*, 2003, **15**, 1535.

59 J. Mei, Y. Hong, J. W. Y. Lam, A. Qin, Y. Tang and B. Z. Tang, *Adv. Mater.*, 2014, **26**, 5429.

60 Y. Dong, J. W. Lam, A. Qin, J. Sun, J. Liu, Z. Li, J. Sun, H. H. Sung, I. D. Williams, H. S. Kwok and B. Z. Tang, *Chem. Commun.*, 2007, 3255.

61 S. Kim, Q. Zheng, G. S. He, D. J. Bharali, H. E. Pudavar, A. Baev and P. N. Prasad, *Adv. Funct. Mater.*, 2006, **16**, 2317.

62 Y. Liu, S. Chen, J. W. Y. Lam, P. Lu, R. T. K. Kwok, F. Mahtab, H. S. Kwok and B. Z. Tang, *Chem. Mater.*, 2011, **23**, 2536.

63 J. Jin, J. Zhang, L. Zou and H. Tian, *Analyst*, 2013, **138**, 1641.

64 P. B. Pati and S. S. Zade, *RSC Adv.*, 2013, **3**, 13457.

65 Y. Zhao and Z. Zhong, *Org. Lett.*, 2006, **8**, 4715.

66 X. Zhang, X. Zhang, S. Wang, M. Liu, L. Tao and Y. Wei, *Nanoscale*, 2013, **5**, 147.

67 T. Abalos, S. Royo, R. Martinez-Manez, F. Sancenon, J. Soto, A. M. Costero, S. Gil and M. Parra, *New J. Chem.*, 2009, **33**, 1641.

68 A. D. Becke, *J. Chem. Phys.*, 1993, **98**, 5648.

69 W. J. Hehre, R. Ditchfield and J. A. Pople, *J. Chem. Phys.*, 1972, **56**, 2257.

70 S. Grimme, J. Antony, S. Ehrlich and H. Krieg, *J. Chem. Phys.*, 2010, **132**, 154104.

71 T. Yanai, D. P. Tew and N. C. Handy, *Chem. Phys. Lett.*, 2004, **393**, 51.

72 R. Krishnan, J. S. Binkley, R. Seeger and J. A. Pople, *J. Chem. Phys.*, 1980, **72**, 650.

73 J. Tomasi, B. Mennucci and R. Cammi, *Chem. Rev.*, 2005, **105**, 2999.

74 M. J. Frisch, G. W. Trucks, H. B. Schlegel, G. E. Scuseria, M. A. Robb, J. R. Cheeseman, G. Scalmani, V. Barone, B. Mennucci and G. A. Petersson, *et al.*, *Gaussian 09, revision A.2*, Gaussian, Inc., Wallingford CT, 2009.